Article

Enhancing Compressive Strength of Reticulated Porous Alumina by Optimizing Processing Conditions

Sujin Lee [1,2], Chae Young Lee [1], Jang-Hoon Ha [1,*,†], Jongman Lee [1], In-Hyuck Song [1] and Se-Hun Kwon [2,*,†]

1   Ceramics Materials Division, Korea Institute of Materials Science, 797 Changwondaero, Seongsan-gu, Changwon 51508, Gyeongsangnam-do, Korea; adsj1503@kims.re.kr (S.L.); cy916@kims.re.kr (C.Y.L.); jmlee@kims.re.kr (J.L.); sih1654@kims.re.kr (I.-H.S.)
2   School of Materials Science and Engineering, Pusan National University, 2 Busandaehak-ro 63beon-gil, Geumjeong-gu, Busan 46241, Korea
*   Correspondence: hjhoon@kims.re.kr (J.-H.H.); sehun@pusan.ac.kr (S.-H.K.)
†   These authors contributed equally to this work.

Featured Application: Ceramic Membranes.

Abstract: Recently, porous ceramics have received much attention from researchers because of their excellent thermal and chemical stabilities compared to their counterparts (such as porous polymers and metals), despite their inferior mechanical instability. Among the various types of porous ceramics, reticulated porous ceramics have significant industrial potential because of their synergistic high porosity and permeability. However, to the best of our knowledge, there is insufficient data on the processing conditions or preparing optimal reticulated porous alumina. Therefore, we prepared and characterized reticulated porous alumina specimens by controlling various processing conditions, namely average particle size, solid loading, binder, and dispersant. The data obtained were used to assess whether the compressive strength of the reticulated porous alumina could be enhanced and to discuss the potential of these materials for various applications.

Keywords: reticulated porous alumina; processing conditions; pore structure; compressive strength

1. Introduction

Over the past several decades, researchers have extensively investigated porous ceramics [1] because of their highly stable thermal and chemical properties. However, unstable mechanical properties inhibit their applications compared to competing materials such as porous metals and polymers. Among the various types of porous ceramics, reticulated porous ceramics are of particular interest because of their high permeability and low density. Their advantageous properties originate from the fact that reticulated porous ceramics consist of interconnected pore channels, unlike porous ceramic foams that, similar to soap bubbles or beehives, have fewer interconnected pore channels.

Among the various types of highly porous ceramics (porosity ≥ 90%), reticulated porous ceramic prepared by the replica method and porous ceramic foams prepared by the particle-stabilized direct foaming method have closed and open-cell structures, respectively. Reticulated porous ceramics can be prepared by coating a reticulated polyurethane foam (as a sacrificial polymer template) with a slurry consisting of ceramic particles [1]. The ceramic slurry-coated reticulated polyurethane foam is then dried and heat-treated to burn off the reticulated polyurethane foam and sinter the ceramic particles. This results in an open-cell pore structure because the sacrificial polymer template is completely coated with ceramic particles when soaked in the ceramic slurry.

Typical examples of the compressive strength of reticulated porous ceramics such as silicon carbide (SiC), zirconia (ZrO_2), silicon nitride (Si_3N_4), mullite ($3Al_2O_3 \cdot 2SiO_2$), and alumina (Al_2O_3) were already addressed in our previous study [2].

As can be understood from the literature data, the low compressive strength of reticulated porous ceramics prevents their use in industrial applications. The compressive strengths of reticulated porous ceramics are strongly dependent on the pore density (PPI) and the processing conditions. Therefore, if the processing conditions of a reticulated porous ceramic are optimized, an enhanced compressive strength can be achieved when using pre-fixed parameters, such as the pore density of the sacrificial polymer template. Consequently, enhancing the compressive strength of reticulated porous ceramics provides an opportunity to achieve synergy between the open-cell structure and high porosity.

In this work, we considered a reticulated porous alumina that may have an enhanced compressive strength that is higher than that of all other ceramics. Unlike other ceramics such as plate-like pyrophyllite ($Al_2Si_4O_{10}(OH)_2$) [3] and porous, irregularly shaped diatomite ($SiO_2 \cdot nH_2O$) [4], regular, spherical alumina particles can easily form as rigid strut walls for a reticulated porous ceramic, improving compressive strength; this is a unique advantage of alumina. If the overall permeability of a reticulated porous ceramic is more important than its overall compressive strength, permeable strut walls prepared using porous and irregular particles, such as diatomite, are favorable. However, if the overall compressive strength is more important than the overall permeability, it is necessary to use ceramic materials that have high strength when dense. Hence, the dense strut walls of reticulated porous alumina and the inherent high compressive strength of bulk alumina are essential for increasing the overall compressive strength of the ceramics.

The low compressive strength of reticulated porous ceramics can be enhanced by several methods; vacuum infiltration coating [5], dip coating [6], centrifuge coating [7], slurry rheology modification [8], multiple slurry coatings [9,10], and whisker-reinforcement coating [11] have all been used to improve the mechanical stability of these ceramics. However, in this study, the enhancement of compressive strength was confined to the optimization of a conventional replica method by tuning processing conditions; average particle size, binder, solid loading, and dispersant.

Notably, we previously studied the feasibility of enhancing the compressive strength of reticulated porous alumina by adopting optimized processing conditions, including the number of alumina coating layers and heat treatment temperature [10]. Unfortunately, the increase in the compressive strength of the reticulated porous alumina was insufficient to deal with those of typical porous alumina. As a follow-up study, in this report, we address more processing conditions, including the average particle size, solid loading, binder, and dispersant within the alumina slurry, and the relationships between the pore structure and the compressive strength of the reticulated porous alumina are presented. Especially, two types of dispersants were used: DARVAN C-N and Dolapix CE 64) were used. Because, DARVAN C-N is an ammonium salt of polymethacrylic acid and Dolapix CE 64 is a sodium salt of a polycarboxylic acid which have been extensively used to disperse alumina [12–14], cordierite [15], zirconia [16], and silicon nitride particles [17].

2. Materials and Methods

The average particle size of the α–alumina was varied using three types of commercial alumina raw materials: with average particle sizes of (1) <50 nm ("fine", Sigma-Aldrich, St. Louis, MO, USA), (2) 0.26 μm ("intermediate", AKP-30, Sumitomo Chemical, Tokyo, Japan), and (3) 2–4 μm ("coarse", AM-210, Sumitomo Chemical, Japan).

Commercial polyurethane foam (SKB Tech, Ulsan, Korea) with a pore density of 45 PPI was used as a sacrificial template. The dimensions of the polyurethane foam used were 100 mm × 100 mm × 20 mm. An alumina slurry consisting of 150–200 g of alumina (fine, intermediate, and coarse), 100 mL of distilled water as a solvent, 0–15 g of polyvinyl alcohol (PVA) as an organic binder (PVA 500, Junsei Chemical, Tokyo, Japan), and 0–1 g of dispersant (DARVAN C-N, Vanderbilt Minerals, USA or Dolapix CE 64, Zschimmer & Schwarz GmbH Co., Burgstädt, Germany) was used to coat the polyurethane foam.

Prior to coating the polyurethane foam, the alumina slurry was mixed uniformly by ball-milling with alumina balls for 4 h. The viscosity of the alumina slurry was measured

using a rotational rheometer (Discovery HR-1, TA Instruments, New Castle, DE, USA) at 25 °C.

The reticulated porous alumina specimens were fabricated using the conventional replica method. A sacrificial polymer template (polyurethane foam) was fully soaked in the prepared alumina slurry until its strut walls were completely coated with alumina particles. The alumina particle-impregnated polyurethane foam was then squeezed to remove excess alumina slurry and to maintain a thin alumina layer over the struts of the polyurethane foam, before being completely dried for 24 h at 25 °C. Following this, the dried specimens were heat-treated at 400 °C for 1 h to burn off the binder and the polyurethane foam and finally sintered at 1600 °C for 1 h using a box furnace (AJ-SKE1-7, Ajeon Heating Industrial, Namyangju-si, Korea). After sintering, the polyurethane foam coated with alumina slurry was transformed into reticulated porous alumina.

After preparing the reticulated porous alumina, the pore structure of specimens was characterized using scanning electron microscopy (SEM, JSM-5800, JEOL, Tokyo, Japan) and micro-computed tomography (μ-CT, XT H 160, voxel size = 3 μm, Nikon, Tokyo, Japan).

The pore size distribution of the specimens was also analyzed using mercury porosimetry (Autopore IV 9510, Micromeritics, Norcross, GA, USA). After machining samples with dimensions of 20 mm × 20 mm × 20 mm, the compressive strength of the specimens was measured with a fixture using an Instron 4206 testing system (Instron, Norwood, MA, USA).

3. Results

A commercial polyurethane foam (used as a sacrificial polymer template, 45 PPI), and the as-prepared reticulated porous alumina specimen (45 PPI) created using polyurethane foam and alumina slurry are shown in Figure 1a. The sintering temperature of the specimens was 1600 °C.

Generally, the pore density of reticulated porous ceramics that can be practically and easily obtained is less than approximately 45 PPI. Therefore, many researchers have studied reticulated porous ceramics with pore densities of less than 45 PPI. For example, reticulated porous ceramics prepared from various types of ceramic raw materials such as alumina (5 [18] and 20 PPI [19–21]), alumina-zirconia composites (20 PPI) [22], aluminum nitride (20 PPI) [23], zirconia (45 PPI) [24], silicon nitride (10 PPI) [11], silicon carbide (8 PPI [25] and 10 PPI [26]), cordierite (10 PPI) [27], and mullite (20 PPI) [28] have pore density values equal to or lower than 45 PPI.
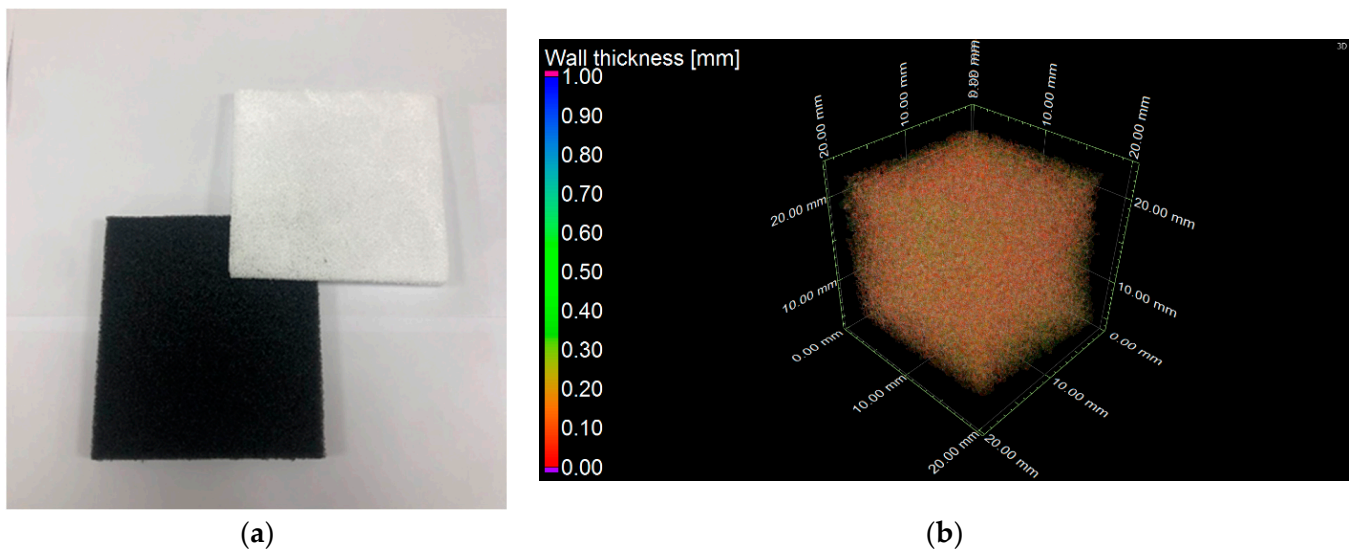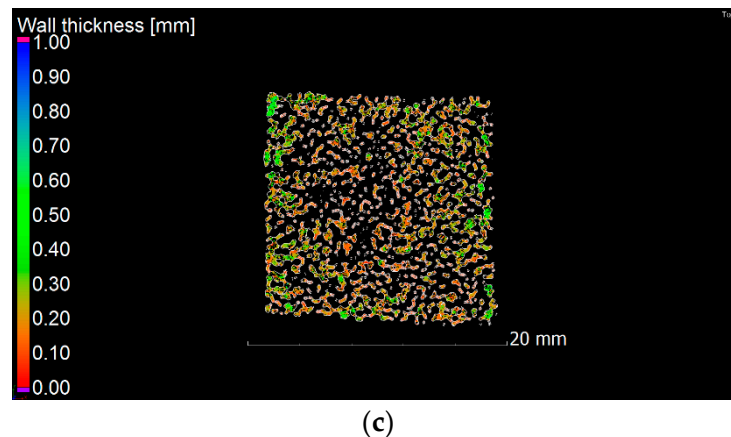

(a)　　　　　　　　　　　　　　　　　　　　　　　　(b)

Figure 1. *Cont.*

(c)

Figure 1. (**a**) Optical images of sacrificial polymer templates (polyurethane foam) (left) and reticulated porous alumina specimen (right) with a pore density of 45 PPI, (**b**) three-dimensional microstructure of typical reticulated porous alumina reconstructed by μ-CT. (**c**) Representative slice extracted from the μ-CT reconstructions.

In this study, the pore density of the reticulated porous alumina specimens was fixed at 45 PPI. This is because the preparation of a reticulated porous ceramic with a pore density of more than 45 PPI is challenging. As the pore density approaches 80 PPI, it would be difficult to entirely coat the strut walls of the sacrificial template as the viscosity of the ceramic slurry increased. Therefore, there would be a narrow margin to optimize various processing conditions, owing to the decreased upper limit of viscosity. Moreover, the compressive strength of reticulated porous alumina with a pore density of 45 PPI is sufficient for practical applications if it can be enhanced further, owing to its dense strut walls.

The main factors governing the properties of a ceramic slurry are the average particle size, solid loading, binder, and dispersant. The required properties of the ceramic slurry depend on the application. Generally, high solid loading and low viscosity are required for applications such as micro-droplet jetting of alumina slurries [29], additive manufacturing of alumina magnesia silicate slurries [30], slip casting of magnesium aluminate spinel slurries [31], additive manufacturing of zirconia toughened alumina slurries [32], and dip coating of cerium oxide slurries [33]. Appropriate solid loading and viscosity are required for the inkjet printing of ceramic ink [34].

In this study, to enhance the compressive strength of reticulated porous alumina, alumina slurries with high solid loading and moderate viscosity were prepared. If the viscosity of the alumina slurry is not high enough, the amount of adsorbed alumina particles in the strut walls of the polyurethane foam would be insufficient, even with a high solid loading. Thus, it cannot completely cover the strut walls of the sacrificial polymer template, which can lead to many defects. Consequently, the overall compressive strength is low.

If the solid loading of the alumina slurry is not high enough, the densification of the strut walls will be insufficient, even with a high viscosity. This results in excessive porosity of the strut walls, which leads to low compressive strength. If the alumina slurry is excessively viscous, it is difficult for it to completely penetrate the polyurethane foam. It is also very difficult to remove excess alumina slurry by squeezing the polyurethane foam while maintaining uniform alumina coating layers over the strut walls.

In general, the viscosity of the alumina slurry increases significantly with increasing solid loading and decreases with increasing average particle size. Hence, to prepare a high solid loading alumina slurry with moderate viscosity, we attempted to determine the optimal processing conditions; especially, solid loading, average particle size, binder, and dispersant. Although several approaches to obtain an extremely high solid loading have been reported by surface modification [35,36], it is beyond the scope of this work.

To vary the average particle size of the alumina particles, fine, intermediate, and coarse alumina was used. An optical image of a commercial polyurethane foam used as a sacrificial polymer template is shown in Figure 1a. Figure 1b shows the three-dimensional microstructure of a typical reticulated porous alumina specimen (pore density = 45 PPI) reconstructed by μ-CT. A representative cross-section of the μ-CT reconstruction of the specimen is shown in Figure 1c. The μ-CT images show that the reticulated porous alumina has highly interconnected pore channels. The image does not show any macrovoids in the strut walls inside the specimen that may have induced by unoptimized processing conditions. Typical SEM images of the as-received fine, intermediate, and coarse alumina particles are shown in Figure 2a–c, respectively. The variation in the average alumina particle size affects the morphology of the strut walls of the reticulated porous alumina as shown in Figure 3a–c.

(a)

(b)

(c)
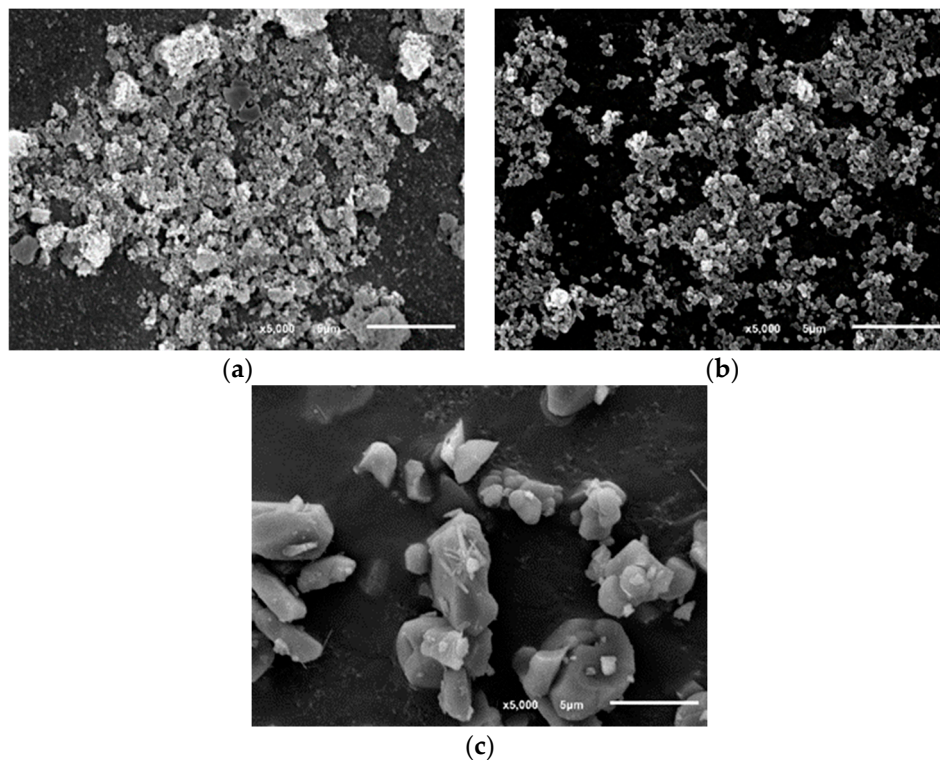
Figure 2. SEM images of as-received alumina particles: (**a**) fine (<50 nm), (**b**) intermediate (0.26 μm), and (**c**) coarse (2–4 μm).


(a)

(b)
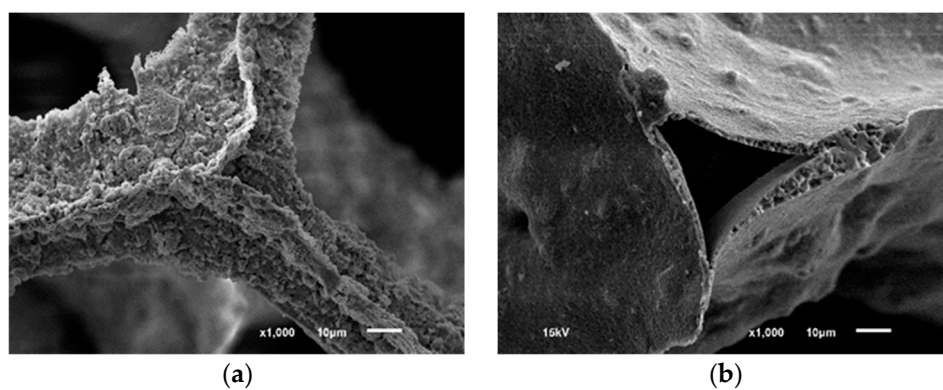
Figure 3. *Cont.*
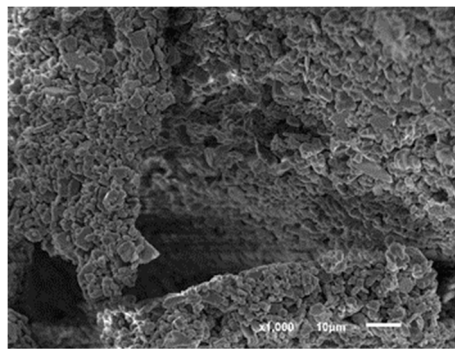
(**c**)

Figure 3. SEM images of fractured strut wall of a reticulated porous alumina specimen prepared from (**a**) fine, (**b**) intermediate, and (**c**) coarse particles.

To determine the feasibility of a reticulated porous alumina for industrial applications and to eliminate nonoptimal processing conditions within the numerous experimental batches, we investigated the effect of the average particle size of the raw materials on the compressive strength of a reticulated porous alumina when all the other processing conditions were fixed. The solid loading, binder, and dispersant have not yet been optimized.

Among the processing conditions that affect the overall processing costs, the cost of ceramic raw materials (which is generally strongly dependent on the average particle size and purity) overwhelms those of other materials, such as binders and dispersants. For example, in this study, the fine: intermediate: coarse cost ratio was approximately 800: 40: 1. Therefore, even if the overall properties of reticulated porous alumina prepared from fine alumina particles are superior, the industrial applications would be severely limited.

Figure 4a shows the compressive strength and density of the reticulated porous alumina specimens prepared from the three average particle sizes, each having a pore density of 45 PPI. The density of the specimens peaked at the intermediate average particle size.
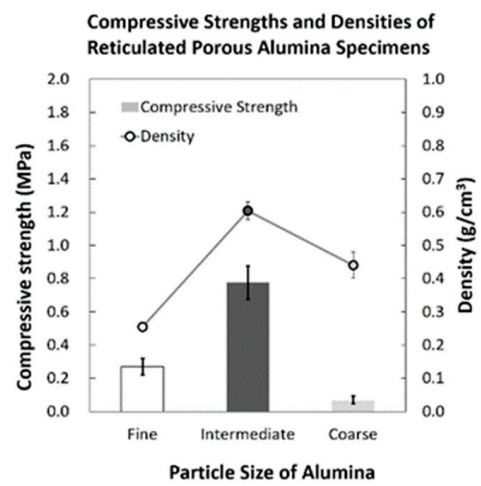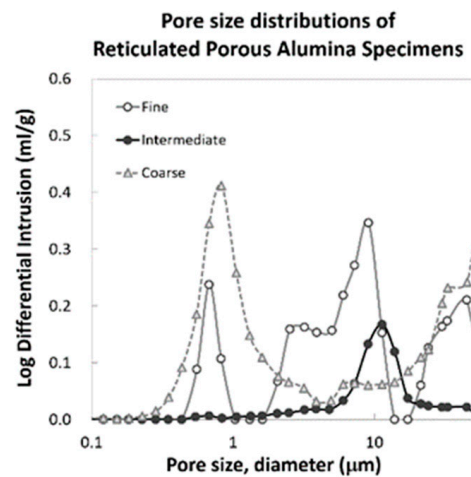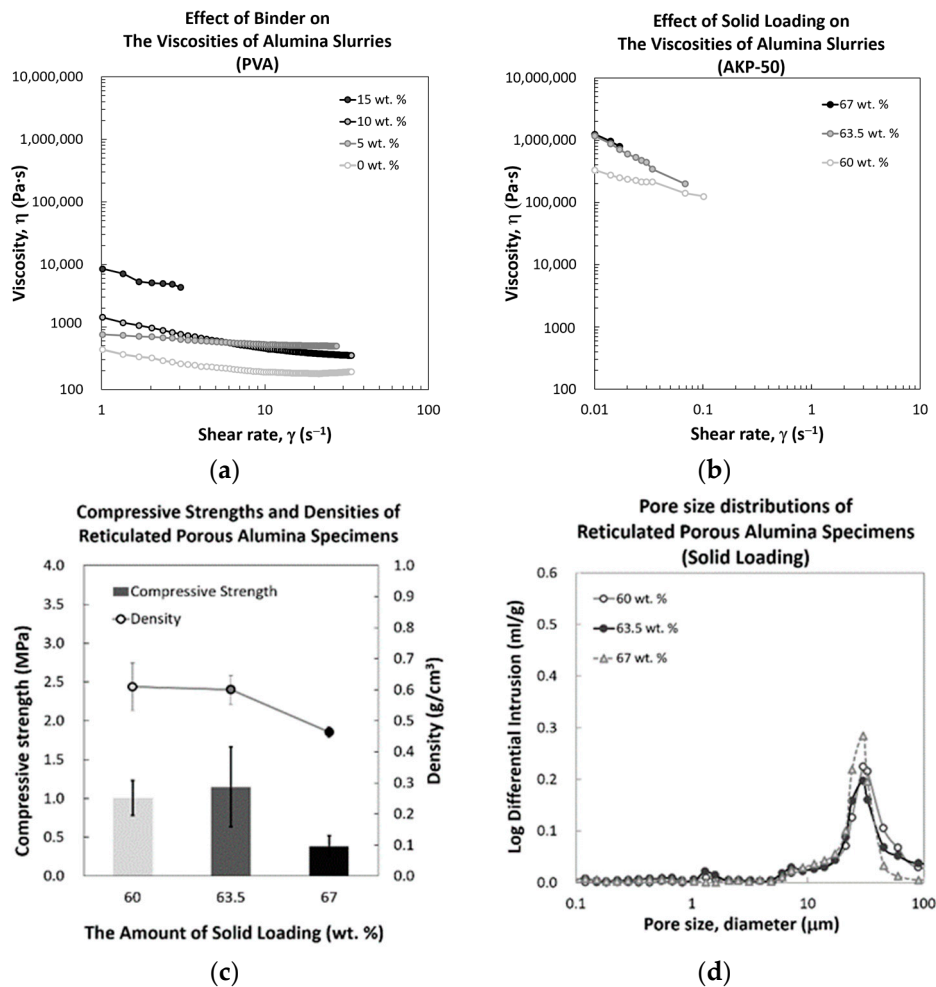

(**a**)
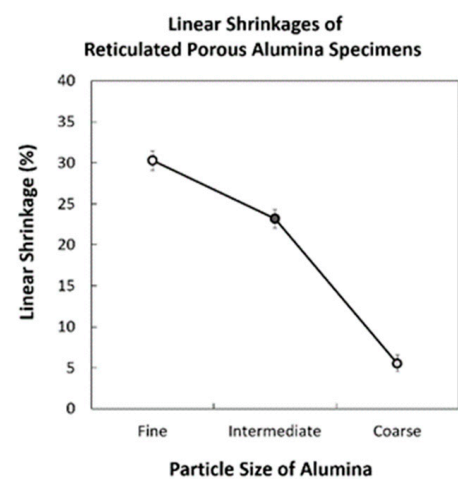
(**b**)

Figure 4. *Cont.*

(**c**)

Figure 4. (**a**) Densities and compressive strengths, (**b**) linear shrinkage, and (**c**) pore size distributions of reticulated porous alumina specimens prepared from fine, intermediate, and coarse alumina particles.

This can be explained as follows. As the average particle size increased, the linear shrinkage of the specimens decreased, as shown in Figure 4b,c depicts the pore size distributions of the reticulated porous alumina specimens (pore density = 45 PPI), prepared using alumina particles of different sizes. For the intermediate alumina, the specimens exhibited a significant decrease in the overall range of pore volume fraction. Because the number of strut walls is invariable and based on the pore density of the polyurethane foam that was used, any difference in the pore size distributions can only be ascribed to the average particle size. The pore size distribution of the reticulated porous alumina prepared from fine alumina particles showed the highest number of pores in the range of 110 μm. This implies that excessive shrinkage during the sintering process, which was induced by nano-sized alumina particles, generated many cracks and defects in the strut walls of the reticulated porous alumina. In contrast, the pore size distribution of the specimen prepared from coarse alumina particles showed the highest number of pores in the range of 0.1 to 1 μm. This indicates that the strut walls of the reticulated porous alumina could not be fully densified by the coarse alumina particles. Because replica processes do not involve conventional cold-isostatic pressing processes, sufficient densification is not achieved when the average particle size is too excessively high.

Therefore, the compressive strength of the specimen prepared from intermediate (0.26 μm) alumina particles was higher than those prepared from fine and coarse alumina particles. Although the absolute value of the compressive strength of reticulated porous alumina has not yet been optimized, (1) we can rule out the use of fine and coarse alumina particles, and (2) we can expect wide industrial applications because of the reasonable raw material cost.

Figure 5a shows a viscosity vs. shear rate plot of the alumina slurries prepared with different amounts of PVA binder at a solid loading of 63.5 wt. %. At 15 wt. % of PVA addition, the viscosity was approximately ten times higher than at 10 wt. %; therefore, the alumina slurry was excessively viscous and could not penetrate into or be squeezed out of the polyurethane foam completely. Figure 5b shows the viscosity vs. shear rate plot of the alumina slurries prepared with different solid loadings with 10 wt. % PVA. Although, we did not expect a further increase in viscosity at a solid loading of over 63.5 wt. %, it was necessary to verify the possibility of increased densification of the strut walls by increasing the amount of solid loading to 67 wt. %.

Figure 5. Viscosity of alumina slurries used for the preparation of reticulated porous alumina: (**a**) 0–15 wt. % of PVA binder with 63.5 wt. % of solid loading, and (**b**) 60–67 wt. % of solid loading with 10 wt. of PVA binder; all other conditions were fixed. (**c**) Density and compressive strength, and (**d**) pore size distributions of reticulated porous alumina specimens prepared from intermediate alumina particles.
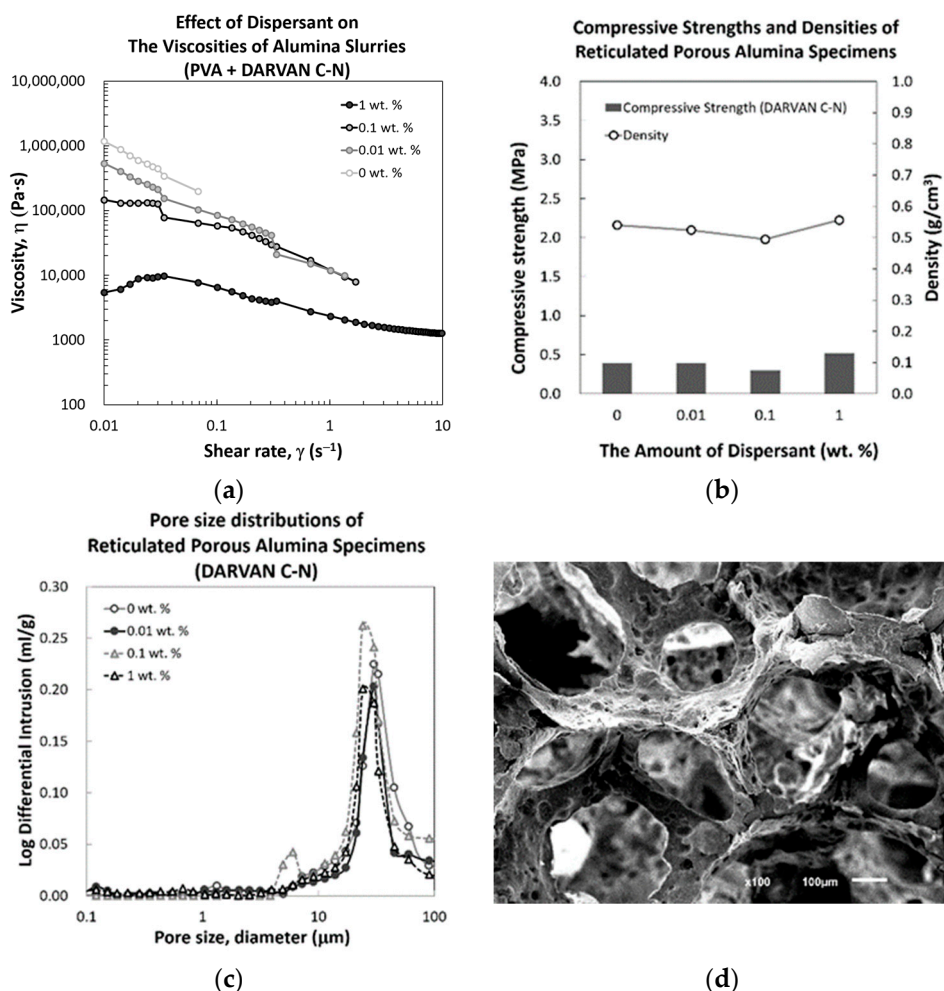
Figure 5c shows the compressive strengths and densities of the reticulated porous alumina specimens prepared with different solid loadings (60 wt. %–67 wt. %). At a solid loading of 63.5 wt.%, the compressive strengths of the specimens peaked, which may be due to the viscosity (Figure 5b). Therefore, using this nonoptimized alumina slurry composition, the effect of the more densified strut walls that were less uniformly coated strut walls (67 wt. %) on the compressive strengths of reticulated porous alumina specimens was inferior to that of the more uniformly coated strut walls that were less densified (63.5 wt. %). We observed large voids and defects generated by the uncoated strut walls of the polyurethane foam deep inside the reticulated porous alumina specimen (at a solid loading of 67 wt. %) due to the high viscosity. At this nonoptimized stage, the excessive solid loading could not induce a further increase in compressive strength.

In Figure 5d, the pore size distributions (ranging from 0.1 to 100 μm) of the strut walls of the specimens prepared from different solid loading can be observed. Although there is a negligible difference in the micron to sub-micron range, which represents the degree of densification of the strut walls, there is a noticeable change in the 10–100 μm range which represents the voids and defects generated by the non-uniformly coated sacrificial polymer template due to the high viscosity. As expected from the values of compressive strengths and densities of the reticulated porous alumina specimens shown in Figure 5c, the pore volume of the reticulated porous alumina specimen prepared at 67 wt. % solid loading was the highest among all the specimens.

We are aware that the amount of PVA (10 wt. %) and the solid loading (63.5 wt. %) were not a fully-optimized and could be enhanced further by adding an appropriate type and amount of dispersant. However, considering the number of processing variables, the initial batch (10 wt. % of PVA and 63. 5 wt. % of solid loading) was suitable for use in further experiments.

Figure 6a shows a viscosity vs. shear rate plot of the alumina slurries prepared with different amounts of DARVAN C-N dispersant at 10 wt. % of PVA binder addition and 63. 5 wt. % of solid loading. With the addition of 1 wt. % of DARVAN C-N, the viscosity was approximately 100 times lower than with 0 wt. % of DARVAN C-N. Consequently, the alumina slurry would be excessively viscous, and it would not be able to penetrate and be squeezed out of the polyurethane foam completely. However, it should be noted again that the highest compressive strength of the reticulated porous alumina specimen was obtained not when the alumina slurry has the slowest viscosity, but when the alumina slurry has an optimized viscosity. A low viscosity inhibits the adhesion of alumina slurry onto the strut walls of the polyurethane foam and promotes the penetration of the alumina slurry deep inside the polyurethane foam.

Figure 6. (**a**) Viscosities, (**b**) densities and compressive strengths, and (**c**) pore size distributions of alumina slurries with 0–1 wt. % of DARVAN C-N dispersant; all other conditions were fixed. (**d**) Typical SEM image of fractured strut wall of reticulated porous alumina specimen prepared with the addition of DARVAN C-N dispersant.

Figure 6b shows the compressive strengths and densities of the reticulated porous alumina specimens prepared using different amounts of DARVAN C-N dispersant (0–1 wt. %), with all the other processing conditions fixed. When the amount of DARVAN C-N dis-

persant was increased, the viscosity of the alumina slurry decreased (Figure 6a). The compressive strengths and densities of the reticulated porous alumina specimens did not vary significantly with the addition of DARVAN C-N.

This tendency can also be observed in the pore size distributions of the reticulated porous alumina specimens prepared using different amounts of DARVAN C-N dispersant. Pore sizes in the range of 0.1–100 μm were observed because this corresponds to the pore size distribution of the strut walls. There is also a negligible difference in the 10–100 μm range, which represents the voids and defects, regardless of the amount of DARVAN C-N dispersant.

The lowered viscosity with the aid of DARVAN C-N dispersant enabled the alumina slurry (63.5 wt. % of solid loading) to deeply penetrate the polyurethane foam, which can be confirmed because there was no density decrease, as was the case when 67 wt. % of solid loading was tested (Figure 6c). However, the increase in solid loading did not contribute to the enhancement of the compressive strength of the reticulated porous alumina specimen.

This can be explained by the microstructure of the reticulated porous alumina specimens. Typical SEM images of the specimens prepared with DARVAN C-N dispersant are shown in Figure 6d. Many defects and non-uniform agglomerates can be observed in the strut walls, which has a negative effect on the overall compressive strength of the specimen, explaining the negligible effect of the DARVAN C-N dispersant. Therefore, for the investigation of the properties of reticulated porous alumina specimens, it is necessary to carefully analyze the densities, compressive strengths, pore size distributions, μ-CT images, and SEM microstructures of the specimens, because these data are all complementary. To further n investigate further the effect of dispersant, we introduced Dolapix CE 64 dispersant which is also well-known as a good dispersant to alumina particles to compare DARVAN C-N dispersant.

Figure 7a shows the viscosity vs. shear rate plot of the alumina slurries prepared with different amounts of Dolapix CE 64 dispersant at 10 wt. % of PVA binder addition and 63. 5 wt. % of solid loading. With the addition of 1 wt. % of Dolapix CE 64, the viscosity of the slurry was approximately ten times lower than at 0 wt. %. Although the effect of the addition of Dolapix CE 64 is similar to that of DARVAN C-N dispersant. Consequently, the alumina slurry would be excessively viscous and would not be able to penetrate and squeeze out of the polyurethane foam completely. However, it should be noted again that the highest compressive strength of the reticulated porous alumina specimen was not obtained when the alumina slurry had the lowest viscosity, but when the alumina slurry had an optimized viscosity. A low viscosity both inhibits the adhesion of alumina slurry onto the strut walls of the polyurethane foam and promotes the penetration of the alumina slurry deep inside the polyurethane foam.
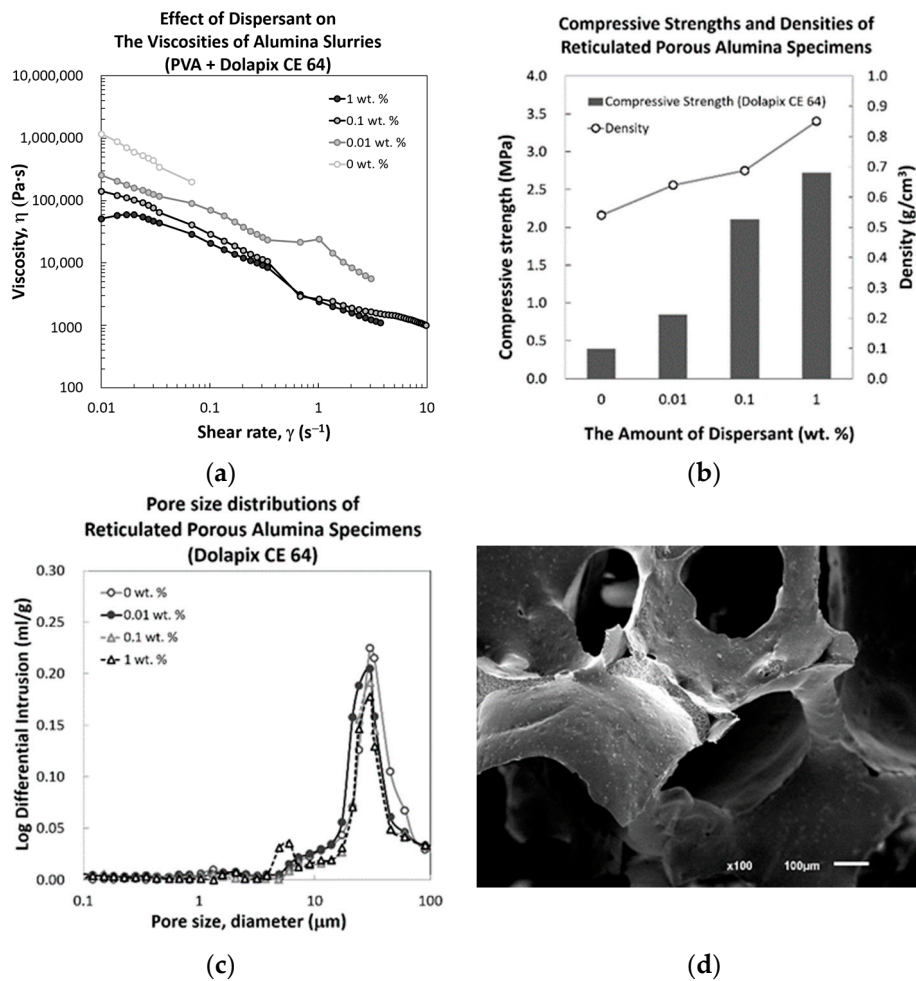
Figure 7. (**a**) Viscosities, (**b**) densities and compressive strengths, and (**c**) pore size distributions of alumina slurries with 0–1 wt. % of Dolapix CE 64 dispersant; all other conditions were fixed. (**d**) Typical SEM image of fractured strut wall of reticulated porous alumina specimen prepared with the addition of Dolapix CE 64 dispersant.

Figure 7b shows the compressive strengths and densities of the reticulated porous alumina specimens prepared using different amounts of Dolapix CE 64 dispersant (0–1 wt. %) with the other processing conditions fixed. Unlike the case of the DARVAN C-N dispersant, the compressive strengths and densities of the reticulated porous alumina specimens significantly increased as the amount of Dolapix CE 64 increased. This can be explained by the pore size distributions of the reticulated porous alumina specimens prepared using different amounts of Dolapix CE 64 dispersant (0–1 wt. %). There is also a negligible difference in the 10–100 μm range, which represents the voids and defects, regardless of the amount of Dolapix CE 64 dispersant.

4. Discussion

In summary, the highest compressive strength of reticulated porous alumina can be obtained when all the aforementioned conditions are satisfied. Although the specimen needs to have the lowest pore volume in the range of 0.1–100 μm (the degree of densification of the strut walls), the range pore volumes above 100 μm (the degree of interconnectivity of pore channels) needs to be chosen appropriately to obtain high permeability, as designed by the PPI of the sacrificial polymer template.

If the average particle size of alumina particles is highly coarse, the densification of the strut walls would be insufficient, which would result in a low compressive strength. In contrast, if the average particle size of alumina is excessively fine, the driving force of sintering will increase significantly, and excessive shrinkage would generate cracks

and defects in the strut walls, which would lead to low compressive strength. For a highly viscous alumina slurry, the highest density cannot be achieved because of the macro voids generated by uncoated areas deep within the polyurethane foam. In contrast, a low viscosity results in a thin strut wall that cannot maintain structural rigidity.

The surface of the specimen had a uniform and defect-free strut walls. This cannot be confirmed by density measurements. The convex shape of alumina agglomerates attached to the strut walls and the concave shape of defects in the strut walls generally complement the overall density of the specimen. Therefore, it needs to be identified using SEM micrography.

5. Conclusions

Reticulated porous alumina specimens were prepared by a conventional replica method using sacrificial polymer templates. The effects of the parameters of the alumina slurry (average particle size, binder, solid loading, and dispersant) on the densities, pore size distributions, and the consequent compressive strengths of the reticulated porous alumina were studied. The experimental results explained the relationships between the properties of the reticulated porous alumina and the processing conditions as follows.

The intermediate alumina particles, 63.5 wt. % of solid loading, and 10 wt. % of PVA binder contributed to the higher density of $0.60 \, \text{g/cm}^3$ from a reticulated porous alumina specimen. Accordingly, increased compressive strength of 0.78 MPa can be obtained. These partially optimized processing conditions are not sufficient to ensure the highest density and the thickest coating of the strut walls without macrovoids within the reticulated porous alumina specimen, and a further increase can be expected with the aid of a dispersant. Although the addition of a dispersant to an alumina slurry may help reduce the viscosity of the slurry, it does not always result in the highest density of the reticulated porous alumina. Only the appropriate type and amount of dispersant will increase the overall compressive strength with uniform and defect-free surfaces of the strut walls of the reticulated porous alumina.

In this study, the novel optimized processing conditions consisted of a slurry composition (average particle size of 0.26 μm, 63.5 wt. % of solid loading, 10 wt. % of PVA binder, 1 wt. % of Dolapix CE 64 dispersant), and sintering conditions (45 PPI and 1600 °C) that can be used to obtain the highest density ($0.85 \, \text{g/cm}^3$) and a compressive strength of 2.72 MPa from a reticulated porous alumina specimen.

Author Contributions: J.-H.H. and S.-H.K. conceived and designed the experiments; S.L. and C.Y.L. performed the experiments; J.L. and J.-H.H. analyzed the data; I.-H.S. contributed reagents/materials/analysis tools; S.L. wrote the paper. All authors have read and agreed to the published version of the manuscript.

References

1. Studart, A.R.; Gonzenbach, U.T.; Tervoort, E.; Gauckler, L.J. Processing Routes to Macroporous Ceramics: A Review. *J. Am. Ceram. Soc.* **2006**, *89*, 1771–1789. [CrossRef]
2. Lee, S.; Lee, C.Y.; Ha, J.H.; Lee, J.; Song, I.H.; Kwon, S.H. Effect of processing conditions on the properties of reticulated porous diatomite–kaolin composites. *Appl. Sci.* **2020**, *10*, 7297. [CrossRef]

3.   Ha, J.-H.; Lee, S.; Abbas Bukhari, S.Z.; Lee, J.; Song, I.-H. The preparation and characterization of alumina-coated pyrophyllite-diatomite composite support layers. *Ceram. Int.* **2017**, *43*, 1536–1542. [CrossRef]

4.   Lee, S.; Ha, J.-H.; Lee, J.; Song, I.-H.; Kwon, S.-H. Preparation and Characterization of a Low-Cost and Natural Material-Based Reticulated Porous Diatomite-Kaolin Composite. *Appl. Sci.* **2020**, *10*, 2125. [CrossRef]

5.   Liang, X.; Li, Y.; Liu, J.; Sang, S.; Chen, Y.; Li, B.; Aneziris, C.G. Improvement of the mechanical properties of SiC reticulated porous ceramics with optimized three-layered struts for porous media combustion. *Ceram. Int.* **2017**, *43*, 3741–3747. [CrossRef]

6.   Touzin, M.; Béclin, F. Fabrication and characterization of composite sol–gel coatings on porous ceramic substrate. *J. Eur. Ceram. Soc.* **2011**, *31*, 1661–1667. [CrossRef]

7.   Pu, X.; Liu, X.; Qiu, F.; Huang, L. Novel method to optimize the structure of reticulated porous ceramics. *J. Am. Ceram. Soc.* **2004**, *87*, 1392–1394. [CrossRef]

8.   Voigt, C.; Aneziris, C.G.; Hubálková, J. Rheological Characterization of Slurries for the Preparation of Alumina Foams via Replica Technique. *J. Am. Ceram. Soc.* **2015**, *98*, 1460–1463. [CrossRef]

9.   Zhu, X.; Jiang, D.; Tan, S.; Zhang, Z. Improvement in the Strut Thickness of Reticulated Porous Ceramics. *J. Am. Ceram. Soc.* **2001**, *84*, 1654–1656. [CrossRef]

10.   Ha, J.-H.; Lee, S.; Choi, J.R.; Lee, J.; Song, I.-H.; Chung, T.-J. A cobalt-coated reticulated porous alumina for radar-absorption applications. *J. Aust. Ceram. Soc.* **2019**, *55*, 883–891. [CrossRef]

11.   Yue, H.; Wang, X.; Tian, J. Fabrication of Si_3N_4 reticulated porous ceramics reinforced by needle-like β-Si_3N_4. *Ceram. Int.* **2014**, *40*, 8525–8532. [CrossRef]

12.   Gaydardzhiev, S.; Ay, P. Characterisation of aqueous suspensions of fumed aluminium oxide in presence of two Dolapix dispersants. *J. Mater. Sci.* **2006**, *41*, 5257–5262. [CrossRef]

13.   Singh, B.P.; Bhattacharjee, S.; Besra, L.; Sengupta, D.K. Evaluation of dispersibility of aqueous alumina suspension in presence of Darvan C. *Ceram. Int.* **2004**, *30*, 939–946. [CrossRef]

14.   Luyten, J.; Thijs, I.; Vandermeulen, W.; Mullens, S.; Wallaeys, B.; Mortelmans, R. Strong ceramic foams from polyurethane templates. *Adv. Appl. Ceram.* **2005**, *104*, 4–8. [CrossRef]

15.   Mei, S.; Yang, J.; Ferreira, J.M.F. Effect of dispersant concentration on slip casting of cordierite-based glass ceramics. *J. Colloid Interface Sci.* **2001**, *241*, 417–421. [CrossRef]

16.   Rao, S.P.; Tripathy, S.S.; Raichur, A.M. Dispersion studies of sub-micron zirconia using Dolapix CE 64. *Colloids Surf. A Physicochem. Eng. Asp.* **2007**, *302*, 553–558. [CrossRef]

17.   Albano, M.P.; Garrido, L.B. Processing of concentrated aqueous silicon nitride slips by slip casting. *J. Am. Ceram. Soc.* **1998**, *81*, 837–844. [CrossRef]

18.   Banerjee, A.; Bala Chandran, R.; Davidson, J.H. Experimental investigation of a reticulated porous alumina heat exchanger for high temperature gas heat recovery. *Appl. Therm. Eng.* **2015**, *75*, 889–895. [CrossRef]

19.   Rannabauer, S.; Söffker, G.M.; Scheunemann, M.; Betke, U.; Scheffler, M. Increased Mechanical Stability and Thermal Conductivity of Alumina Reticulated Porous Ceramics (RPC) by Nanoparticle Infiltration Processing. *Adv. Eng. Mater.* **2017**, *19*, 1700211. [CrossRef]

20.   Voigt, C.; Zienert, T.; Schubert, P.; Aneziris, C.G.; Hubálková, J. Reticulated porous foam ceramics with different surface chemistries. *J. Am. Ceram. Soc.* **2014**, *97*, 2046–2053. [CrossRef]

21.   Voigt, C.; Jäckel, E.; Aneziris, C.G.; Hubálková, J. Investigations of reticulated porous alumina foam ceramics based on different coating techniques with the aid of μCT and statistical characteristics. *Ceram. Int.* **2013**, *39*, 2415–2422. [CrossRef]

22.   Chen, R.; Jia, W.; Wang, Y.; Lao, D.; Hei, D.; Li, S. Optimization of the microstructure and properties of Al_2O_3-ZrO_2 reticulated porous ceramics via in-situ synthesis of mullite whiskers and flowing-liquid phase. *Mater. Lett.* **2019**, *243*, 66–68. [CrossRef]

23.   Betke, U.; Lieb, A.; Scheffler, F.; Scheffler, M. Manufacturing of Reticulated Open-Cellular Aluminum Nitride Ceramic Foams from Aqueous AlN Suspensions. *Adv. Eng. Mater.* **2016**, *19*, 1600660. [CrossRef]

24.   Jun, I.-K.; Koh, Y.-H.; Song, J.-H.; Lee, S.-H.; Kim, H.-E. Improved compressive strength of reticulated porous zirconia using carbon coated polymeric sponge as novel template. *Mater. Lett.* **2006**, *60*, 2507–2510. [CrossRef]

25.   Yao, X.; Tan, S.; Huang, Z.; Jiang, D. Effect of recoating slurry viscosity on the properties of reticulated porous silicon carbide ceramics. *Ceram. Int.* **2006**, *32*, 137–142. [CrossRef]

26.   Liang, X.; Li, Y.; Sang, S.; Xu, Y.; Chen, Y.; Li, B.; Aneziris, C. Enhanced mechanical properties of SiC reticulated porous ceramics via adjustment of residual stress within the strut. *Int. J. Appl. Ceram. Technol.* **2018**, *15*, 28–35. [CrossRef]

27.   Biswas, P.; Varaprasad, K.; Ramavath, P.; Suresh, M.B.; Khanra, A.K.; Johnson, R. Development of Cordierite Based Reticulated Foams with Improved Mechanical Properties for Porous Burner Applications. *Trans. Indian Ceram. Soc.* **2017**, *76*, 56–61. [CrossRef]

28.   Akpinar, S.; Altun, I.A.; Onel, K. Effects of SiC addition on the structure and properties of reticulated porous mullite ceramics. *J. Eur. Ceram. Soc.* **2010**, *30*, 2727–2734. [CrossRef]

29.   Cai, J.; Fan, S.; Liu, F.; Jiang, W.; Wu, H.; Fan, Z. Preparation of porous Al_2O_3 ceramic microspheres by a novel micro-droplet jetting rapid forming method. *Ceram. Int.* **2019**, *45*, 20583–20588. [CrossRef]

30.   Chen, Z.; Li, J.; Liu, C.; Liu, Y.; Zhu, J.; Lao, C. Preparation of high solid loading and low viscosity ceramic slurries for photopolymerization-based 3D printing. *Ceram. Int.* **2019**, *45*, 11549–11557. [CrossRef]

31.   Shafeiey, A.; Enayati, M.H.; Al-Haji, A. The effect of slip casting parameters on the green density of $MgAl_2O_4$ spinel. *Ceram. Int.* **2017**, *43*, 6069–6074. [CrossRef]

32. Xing, H.; Zou, B.; Liu, X.; Wang, X.; Chen, Q.; Fu, X.; Li, Y. Effect of particle size distribution on the preparation of ZTA ceramic paste applying for stereolithography 3D printing. *Powder Technol.* **2020**, *359*, 314–322. [CrossRef]

33. Balzarotti, R.; Cristiani, C.; Latorrata, S.; Migliavacca, A. Washcoating of low surface area cerium oxide on complex geometry substrates. *Part. Sci. Technol.* **2016**, *34*, 184–193. [CrossRef]

34. Güngör, G.L.; Kara, A.; Gardini, D.; Blosi, M.; Dondi, M.; Zanelli, C. Ink-jet printability of aqueous ceramic inks for digital decoration of ceramic tiles. *Dyes Pigm.* **2016**, *127*, 148–154. [CrossRef]

35. Liu, W.; Jin, L.; Wang, S. Preparation of transparent Y_2O_3 ceramic via gel casting: Realization of high solid volume via surface modification. *J. Am. Ceram. Soc.* **2019**, *102*, 6414–6421. [CrossRef]

36. Gao, X.; Wang, R.; Zhao, J.; Huang, J.; Gao, Y.; Liu, H. Influence of surface oxide layer of SiC powder on the rheological properties of its slurry. *Int. J. Appl. Ceram. Technol.* **2020**, *17*, 484–490. [CrossRef]